Expanded View Figures

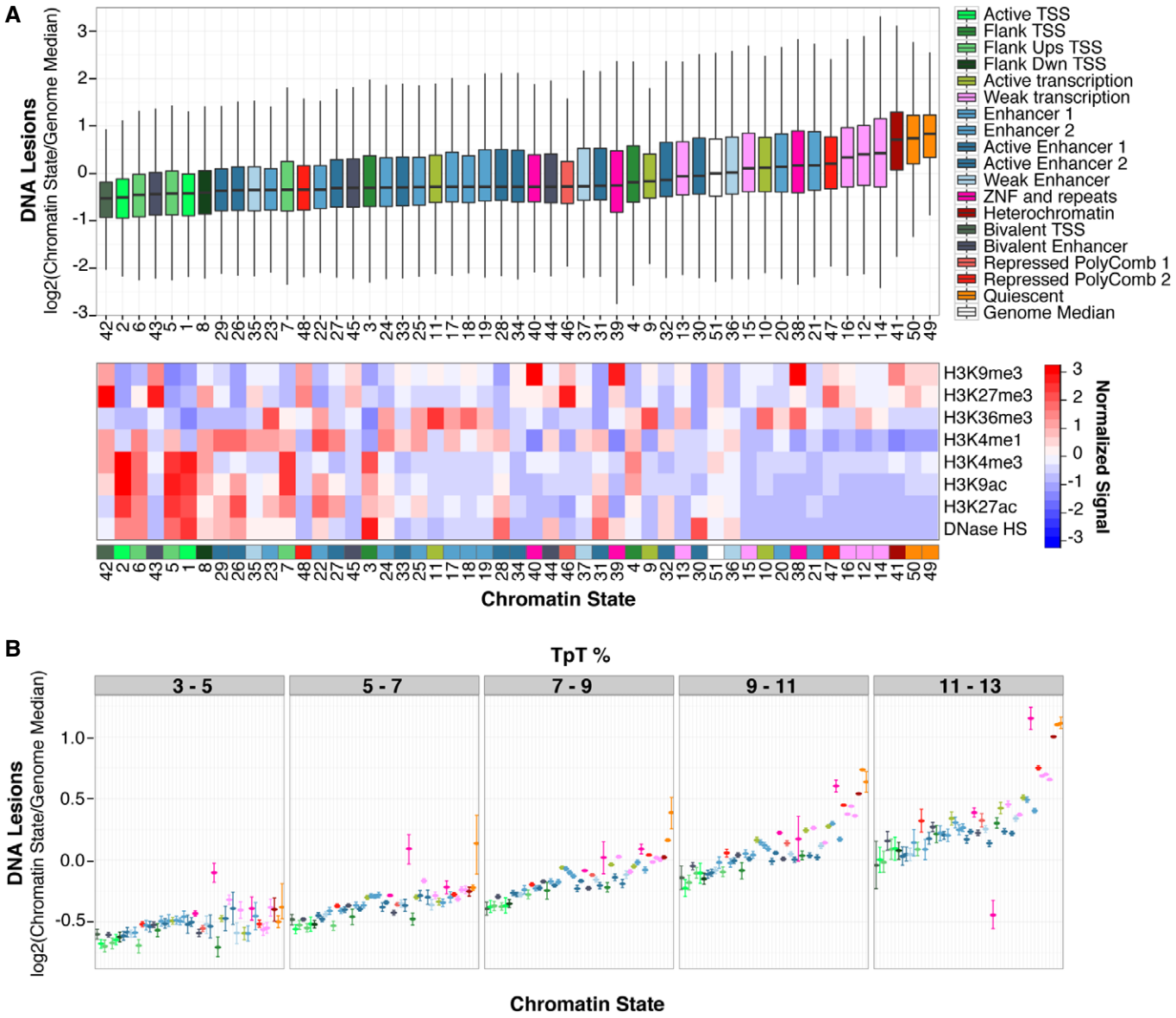

Figure EV1. Heterochromatic states are susceptible to the UV carcinogen.

A Same as in Fig 1, except UV lesion abundance was measured within 50 different chromatin states constructed with all IMR90 chromatin marks available in the Roadmap Epigenomics project (Roadmap Epigenomics Consortium *et al*, 2015). Multiple chromatin states are assigned to individual functional categories. Statistical outliers are omitted.

B UV lesion abundance was calculated as in (A) after binning by TpT content. Error bars denote the 95% confidence interval of the mean based on bootstrapping 1,000 times.

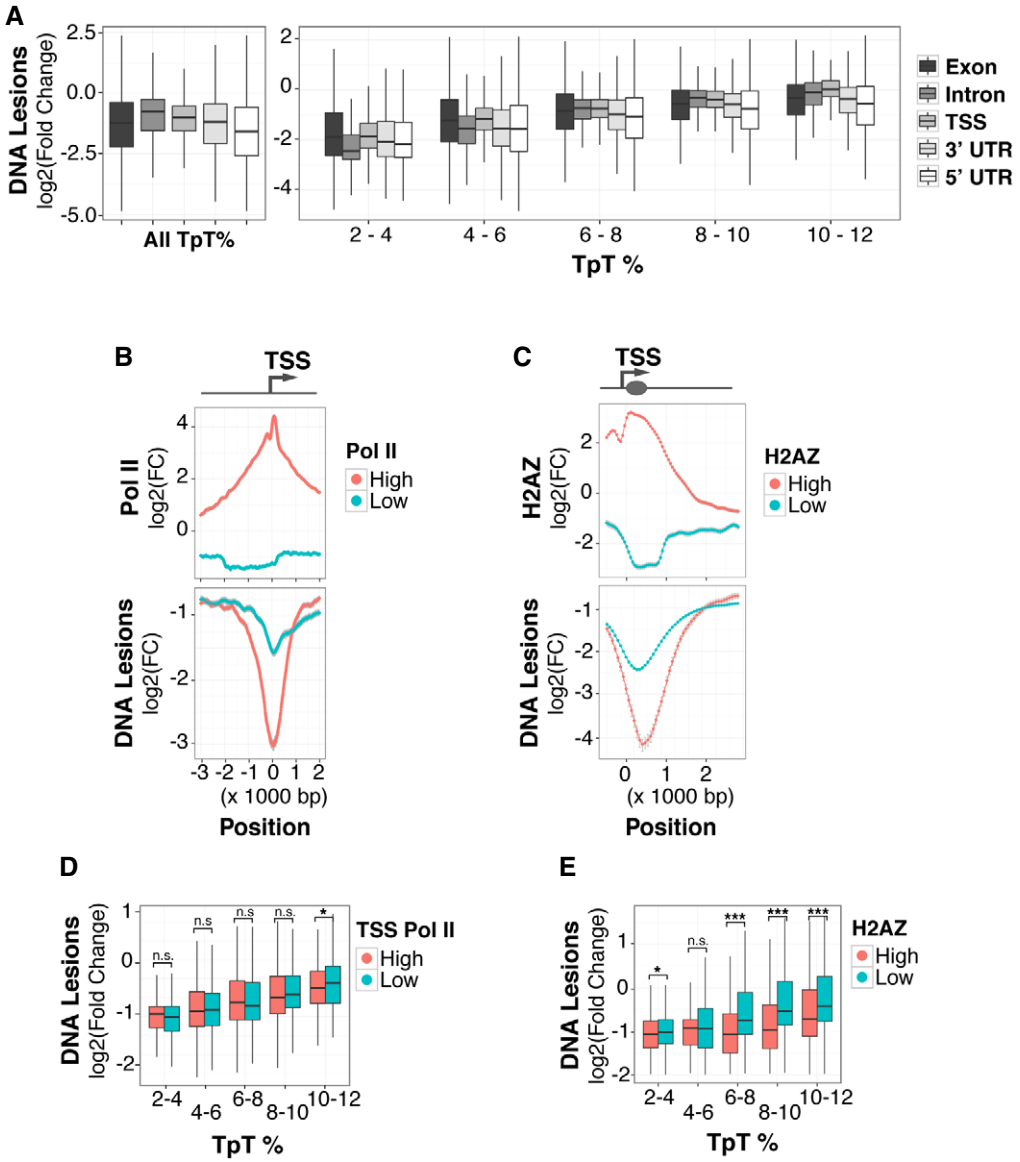

Figure EV2. Specific genic features are protected against UV-induced lesions.

A Abundance of UV lesions (IP/input) within genic features of annotated protein-coding genes binned according to TpT frequency. Transcriptional start site and untranslated region are abbreviated as TSS and UTR, respectively. Middle quartiles are represented by boxes, top and bottom quartiles are represented by whiskers.

B UV lesion abundance at TSSs with high (top 10%) and low Pol II occupancy (bottom 10%).

C UV lesion abundance at genes with high (top 5%) or low H2AZ occupancy (bottom 5%).

D, E UV lesion abundance calculated after binning by TpT content for TSSs (D) and H2AZ-containing TSSs (E). Mann–Whitney test $*P < 0.05$, $***P < 0.001$, or not significant (n.s.). Outliers are omitted for all boxplots. Middle quartiles are represented by boxes, top and bottom quartiles are represented by whiskers.

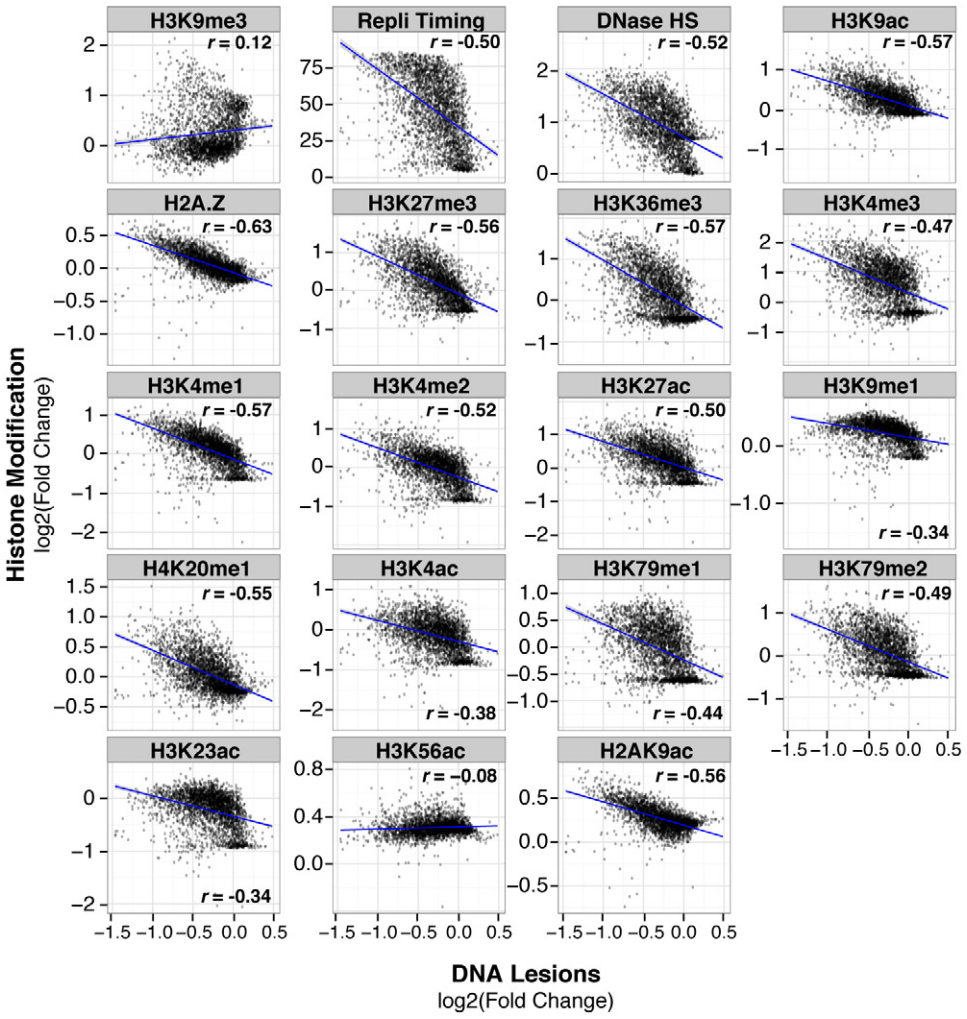

Figure EV3. UV susceptibility negatively correlates with replication timing and euchromatic histone modifications.

DNA lesions abundance (IP/input) quantified within 1-Mb windows compared to abundance of histone modifications previously identified (Roadmap Epigenomics Consortium *et al*, 2015). Pearsons correlation is shown, and linear regression line (blue) with its associated standard deviation (gray) was fitted to the data. $P < 0.001$ for all graphs.

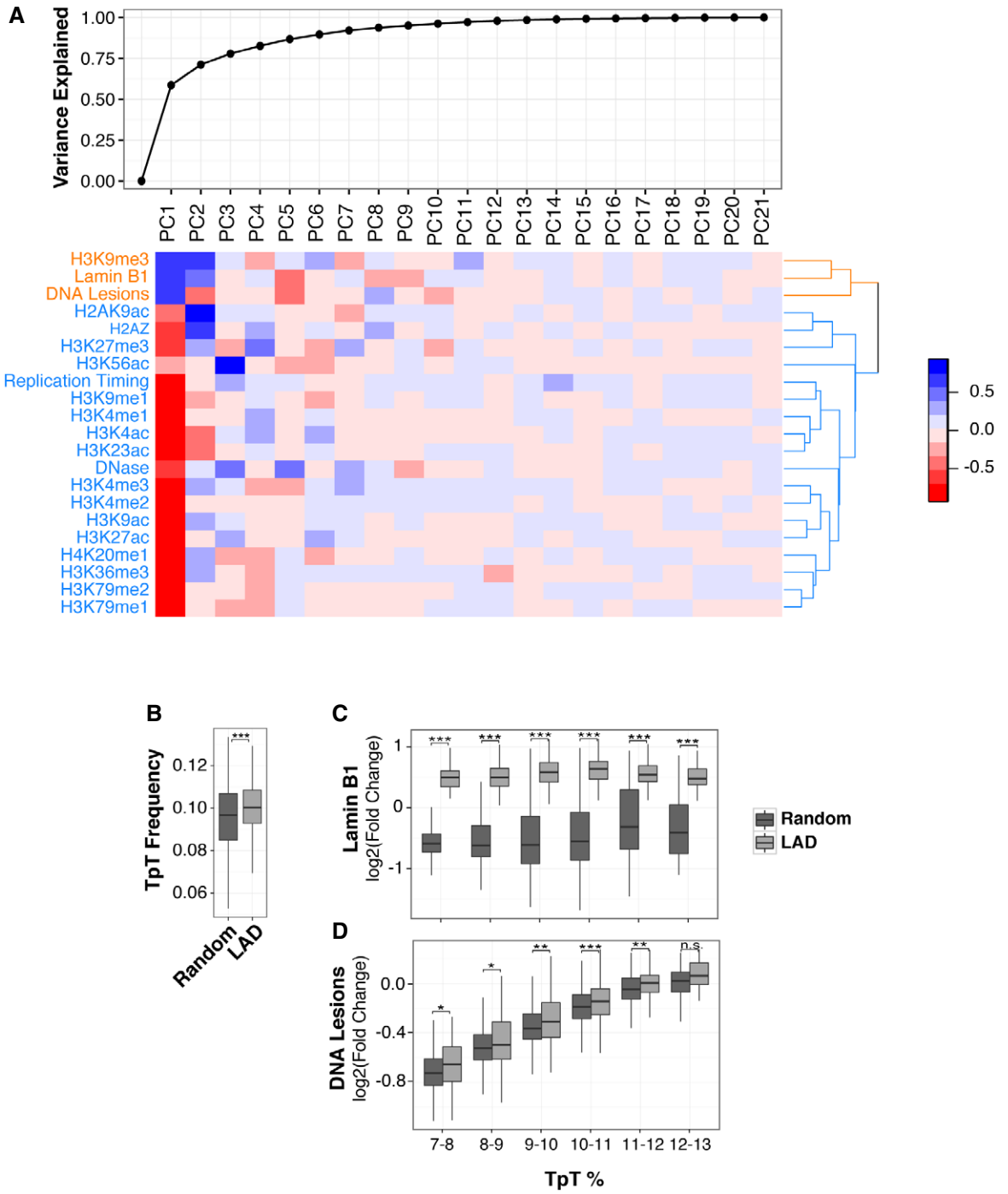

Figure EV4. UV susceptibility is correlated with heterochromatin and lamin B1 and is not sequence-dependent.

A Principal component analysis was performed with the indicated features at a 1-Mb scale (refer to Materials and Methods for more details). Top, cumulative variance explained by all principal components (PCs). Bottom, the correlation heatmap is shown. Rows in heatmap were reordered based on a hierarchical clustering using Euclidean distance.

B The TpT content of LADs and randomly selected regions of equal size.

C Lamin B1 abundance distribution in LADs and a random control after binning based on TpT dinucleotide content.

D DNA lesion signal distribution (IP/input) in same groups as in (B). Random control was generated by arbitrarily sampling non-LAD regions of the genome of the same number, size, and chromosomal distribution of LADs.

Data information: (B–D) Statistical outliers are omitted. Mann–Whitney test *$P < 0.05$, **$P < 0.01$, ***$P < 0.001$, or not significant (n.s.).

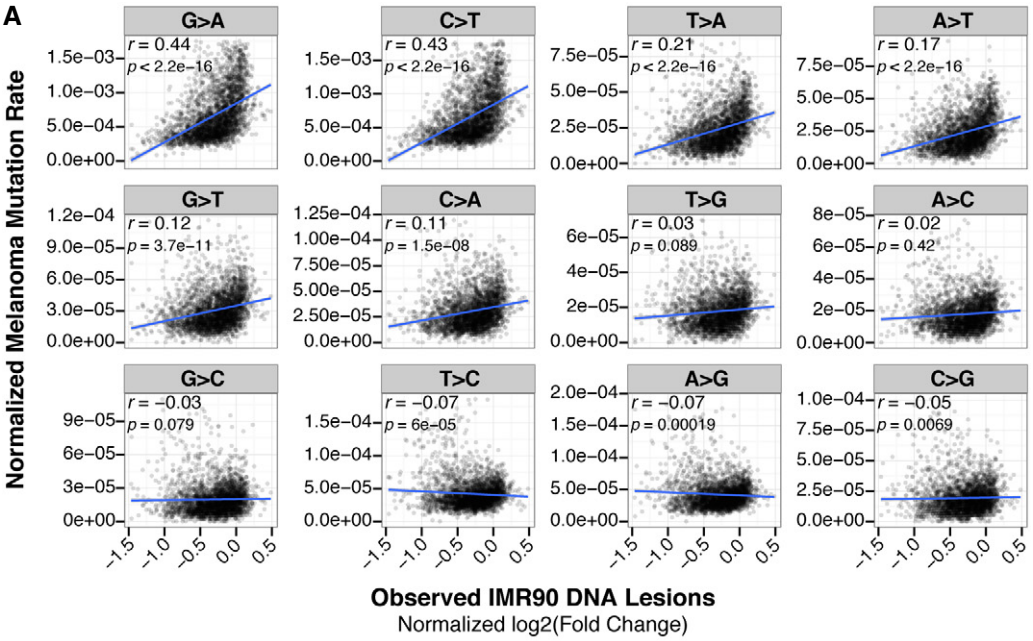

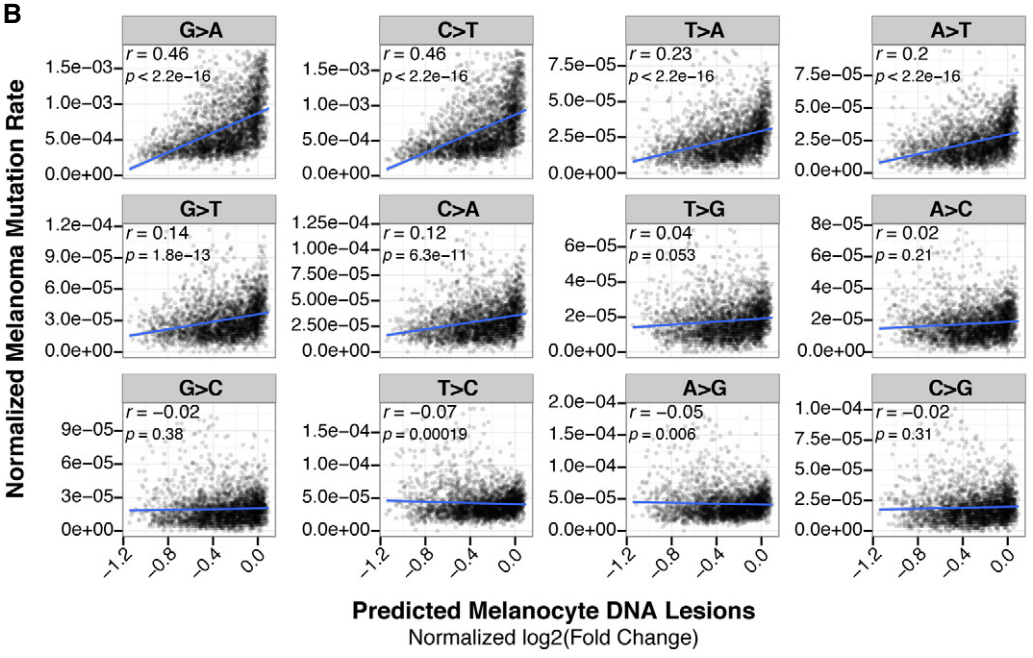

Figure EV5. Correlation between UV-induced DNA lesions and mutation frequency in melanoma.

A, B Genome-wide mutation frequency in melanoma compared to UV lesion abundance (IP/input) observed in IMR90 cells (A), and predicted in melanocytes (B). *Y*-axes are truncated at the 99th percentile.

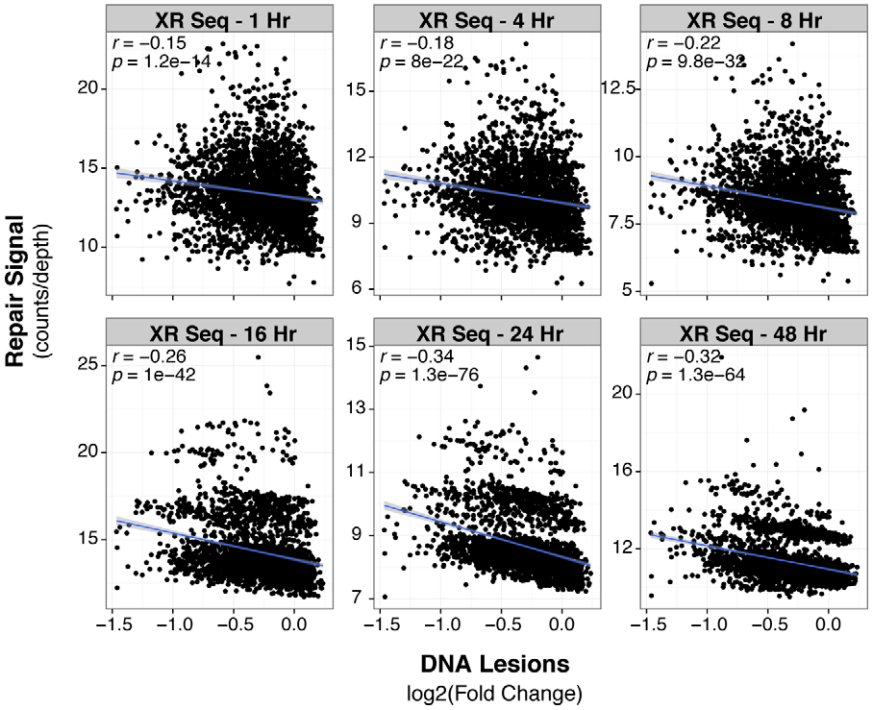

Figure EV6. UV susceptible regions of the genome have less efficient excision repair.

Comparison across all 1-Mb windows of the genome between DNA lesions (fold change of IP/input) and excision repair rates measured by XR-seq at indicated time points (Adar *et al*, 2016). Pearson correlation (*r*) and its associated *P*-value (*P*) are shown.